A New Solvent Mixture for use of LiTDI as Electrolyte Salt in Li-ion Batteries

Christopher L. Berhaut[a,c], Remi Dedryvère[b], Laure Timperman[a], Grégory Schmidt[c], Daniel Lemordant[a], Mériem Anouti[a]*

(a) Laboratoire PCM2E (EA 6296), UFR Sciences et Techniques, Université François Rabelais de Tours, Parc de Grandmont, 37200 TOURS, France

(b) IPREM, Université de Pau, Hélioparc Pau Pyrénées, 2 av. Pierre Angot, 64053 Pau Cedex9, France

(c) ARKEMA, rue Henri Moissan, 69493 Pierre Bénite, France

(*) ISE active member

Email: christopher.berhaut@outlook.com

Keywords: Li-ion batteries, 4,5-dicyano-2-(trifluoromethyl)imidazol-1-ide (LiTDI), electrolyte thermal stability, Solid Electrolyte Interphase, salt dissociation.

Abstract

A new thermally stable ternary mixture composed of ethylene carbonate, γ-butyrolactone and methyl propionate (1: 1: 1 by weight), named EGM, is proposed for use as an electrolyte with the new salt LiTDI at a concentration of 1 mol.L^{-1}. The EGM mixture has many advantages over the classical binary mixture EC/DMC (1:1 by weight) when LiTDI is used as single salt: (i) it remains liquid from -60 °C to 130 °C, (ii) it exhibits a higher conductivity (8.5 mS.cm^{-1} vs. 6.8 mS.cm^{-1} at 25 °C), (iii) a lower viscosity (2.4 mPa.s vs. 2.8 mPa.s at 25 °C) and, (iv) allows a better dissociation of LiTDI (37 % vs. 31 %). Cycling tests were performed using graphite/Li and $LiNi_{1/3}Mn_{1/3}Co_{1/3}O_2$ (NMC)/Li half-cells as well as graphite/NMC full cells. It was shown that this electrolyte provides fair capacity retention for both the graphite and the NMC electrode at high C rates: up to 10C for graphite/Li half-cells and up to 6C for NMC/Li half-cells. The graphite//LiTDI-EGM//NMC full cell was able to sustain more than 800 cycles with a capacity retention of 70 %, which is more than what was obtained in the same conditions with a graphite//$LiPF_6$-EC/DMC//NMC cell (560 cycles). The impact on the discharge capacities of high (60 °C) and low (-20 °C) applied temperatures is also discussed herein.

1. Introduction

To keep up with the ever-increasing number of renewable energy generating systems there is a need to improve the battery energy storage. Future batteries should present both a larger energy density and an improved security at lower cost. Lithium-ion batteries (LiB) remain the most suited candidate for this purpose owing to their low weight, low self-discharge and already good electrochemical performances. LiB technology has become popular over the years and today, LiBs are widely used to convert stored chemical energy into electrical energy in portable electronics [1] as well as in larger scale applications such as electric vehicles. Over years, the success of this technology has been largely dependent on the choice of electrode materials and electrolyte formulations [2-4]. Most of the commercial LiBs used in currently available electrical devices contain as electrolyte lithium hexafluorophosphate ($LiPF_6$) dissolved in a mixture of alkylcarbonates. The main reasons for this [3, 5, 6] are the high conductivity of $LiPF_6$ solutions, the formation of a protective solid electrolyte interphase (SEI) on graphite negative electrodes and the ability of $LiPF_6$ to passivate aluminum, a low-cost metal used as current collector for positive electrodes. However, the lack of thermodynamic stability and the moisture sensitivity of $LiPF_6$ induce high risks of releasing HF and/or PF_5 via its thermal decomposition or hydrolysis in the presence of water. These drawbacks have been highly criticized justifying the importance in finding a replacement. The most important function of the electrolyte is charge transportation from one electrode to the other and so the main requirements are: (i) a high ionic conductivity for battery power, (ii) a low viscosity for cell filling, (iii) high electrochemical and chemical stabilities to avoid solvent decomposition and gazing at the electrode interfaces, (iv) no phase change within the working temperature range and, (v) good wetting properties of the separator and the

composite electrodes. Moreover, a large life-span without safety risks, especially when damaged, is highly considered by users and manufacturers.

Owing to its high thermal stability, low sensitivity to the presence of water and electrochemical stability [7], lithium 4,5-dicyano-2-(trifluoromethyl)imidazol-1-ide (LiTDI) is seen as a promising substitute for $LiPF_6$ in LiBs. Recent studies [4, 8] demonstrate that LiTDI is able to protect aluminum from corrosion without releasing HF and can be used with standard cathode material due to its electrochemical stability (up to 4.5 V vs. Li^+/Li) [9]. In alkylcarbonate mixtures like EC/DMC, LiTDI provides reasonable conductivities [8, 10-12] which nevertheless remain lower than that obtained with $LiPF_6$. As a matter of fact, LiTDI is not well dissociated in alkylcarbonates owing to the formation of ion pairs (IP) [13] and possibly larger aggregates. This is the main reason for the lower conductivity of electrolytes containing LiTDI as compared to $LiPF_6$ or other lithium-salts such as lithium tris(pentafluoroethane)-trifluorophosphate (LiFAP), lithium bis(trifluoromethylsulfonyl)imide (LiTFSI) or lithium bis(fluorosulfonyl)imide (LiFSI) [10].

In this work a new ternary mixture is proposed for using LiTDI as an electrolyte lithium salt. This mixture, called EGM in the following, is composed of ethylene carbonate (EC), γ-butyrolactone (GBL) and methyl propionate (MP) in the weight proportions (1: 1: 1). The new LiTDI-EGM electrolyte, EGM in which LiTDI is added at a concentration of 1 $mol.L^{-1}$, will be compared to LiTDI-EC/DMC (1:1 by weight) and $LiPF_6$-EC/DMC (1:1 by weight). $LiPF_6$-EC/DMC has been used as an electrolyte for many purposes and its properties are well described in the literature [6, 14-16]. The following properties will be considered: salt dissociation, electrolyte thermal stability, passivation of aluminum and lithiated graphite (SEI formation). Electrode material capacity retention will be studied within half-cells (graphite (Gr)/Li, $LiNi_{1/3}Mn_{1/3}Co_{1/3}O_2$ (NMC)/Li). Extended cycling will be performed using full NMC/Gr cells. The LiTDI-EGM electrolyte will also be tested under severe operating

conditions, i.e. high (60 °C) and low (-20 °C) temperatures and under high discharge rates (up to 10D).

2. Experimental section

2.1. Battery preparation

Highly pure (GC grade, purity > 99 %) ethylene carbonate (EC), analytical g-butyrolactone (GBL, purity > 99 %), methyl propionate (MP, GC grade, purity > 99 %) and anhydrous dimethylcarbonate (DMC, purity > 99 %) purchased from Sigma-Aldrich, were used as received. The alkyl-carbonate mixture EC/DMC (1: 1, by weight) and the EGM mixture (EC/GBL/MP, 1: 1: 1, by weight) were prepared using a Sartorius 1602 MP balance with an accuracy of ±1 x 10^{-4} g in an argon filled MBraun glove box at 25 °C containing less than 5 ppm of moister and oxygen. A GeneCust desiccant bag was placed in the solvent mixtures to reduce the water content to a minimal level (10 ppm).

Battery grade lithium hexafluorophosphate ($LiPF_6$) purchased from Fluorochem was kept and used under the dry atmosphere of the glove box.

Lithium 4,5-dicyano-2-(trifluoromethyl)imidazol-1-ide (LiTDI) was supplied by Arkema and kept in the glove box. LiTDI and $LiPF_6$ based electrolytes were prepared in the glove box at concentrations ranging from 1 x 10^{-4} mol.L^{-1} to 2 mol.L^{-1} and kept there before use. Concentrations below 1 mol.L^{-1} were obtained by dilution. For cell testing, 2 % by weight of fluoroethylene carbonate (FEC) was added to the electrolytes.

Prior to any measurement, the water content of each electrolyte was measured using an 831 Karl-Fisher Coulometer (Metrohm). The water content of the $LiPF_6$ and LiTDI based electrolytes was respectively lower than 20 ± 1 ppm and 100 ± 1 ppm (due to the high hygroscopic behaviour of LiTDI).

NMC and graphite electrodes are gifts from Arkema and were dried at 90 °C under vacuum for two hours before being stored in the glove box where the CR2032 coin-cells were then prepared.

2.2. Experimental methods

The relative permittivity ε_r of EGM and EC/DMC were obtained through impedance measurements. A two electrode Swagelok® system was filled with a small amount of solvent (≈ 0.1 mL) inside the glove box allowing a thin layer (e ≈ 0.8 mm) of liquid spreading between the two steel connectors.

The capacity C of the cell was determined by impedance measurements performed with an A.C. signal (10 mV) in the frequency range of 500 MHz to 100 mHz with 50 points per decade. The permittivity (ε) and relative permittivity (ε_r) of the mixture were then calculated using equation (1):

$$\varepsilon = \varepsilon_r \, \varepsilon_0 = C \, e/S \qquad \text{Eq. 1}$$

where e is the distance between the two disk electrodes, S the surface area of the disks, C the capacity of the cell and ε_0 the vacuum permittivity (8.854187 x 10^{-12} F.m^{-1}).

Differential Scanning Calorimetry was performed with a PerkinElmer DSC 4000. Samples, initially at 30 °C, were first cooled down to -40 °C and then heated up to 70 °C before being cooled once more down to -60 °C for EC/GBL/MP based electrolytes or -40 °C for EC/DMC based electrolytes and finally heated up to 150 °C. Each scan was performed at 2 °C.min^{-1} and was followed by a 1 minute isothermal plateau.

Conductivity measurements were performed using a BioLogic Multichannel Conductivity Meter based on frequency Response Analyser (MCM 10). Measurements where made using sealed cells with Pt parallel-plate-electrodes protecting the samples from air exposure. For temperature control, the cells were connected to a Peltier based temperature control unit with 10 slots (WTSH 10).

Density and viscosity measurements were carried out from 10 °C to 80 °C using respectively an Anton Parr digital vibrating tube densitometer (model 60/602, Anton Parr, France) and an Anton Parr rolling-ball viscometer (Lovis 2000M/ME, Anton Parr, France). In both cases the cell temperature was regulated within ± 0.02 °C. Dynamic viscosity values reported in this paper were calculated by taking into account the effect of the sample density and the buoyancy of the ball in each sample as a function of the temperature. The densitometer was firstly calibrated at all temperatures with degassed water and dehumidified air at atmospheric pressure as recommended by the constructor while ultra-pure water was used to calibrate the viscometer. The uncertainty of the density and viscosity measurements are better than 5×10^{-5} g.cm^{-3}, and 1 %, respectively.

The salt dissociation coefficient (α_D) was estimated herein using the Walden rule given by equation (2):

$$\frac{\Lambda\,\eta}{\Lambda^{\circ}\eta^{\circ}} = \frac{W}{W^{\circ}} = \alpha_D \qquad \text{Eq. 2}$$

where Λ, Λ°, η and η° are respectively the molar conductivity, the high dilution limit molar conductivity, the medium viscosity and the solvent mixture viscosity. The limiting molar conductivity Λ° values are obtained by extrapolating at high dilution the Debye-Hückel-Onsager equation:

$$\Lambda = \Lambda^{\circ} - S\sqrt[2]{C} \qquad \text{Eq. 3}$$

where S is a constant.

Electrochemical measurements were performed on a MPG2 Biologic multichannel potentiostat at the exception of impedance measurements which were conducted on a VMP3 Biologic multichannel potentiostat.

Half and full-cells were tested using the same galvanostatic procedure with a constant charge rate of C/5 (Gr lithiation, NMC delithiation) and discharge rates ranging from D/24 to 10D.

NMC/Li half-cells and NMC/Gr cells were cycled between 3 V and 4.2 V vs. Li^+/Li and Gr/Li half-cells between 0.01 V and 1 V vs. Li^+/Li.

Electrochemical impedances were obtained using three electrode Swagelok® systems with lithium metal as reference electrode, NMC as counter electrode and Gr as working electrode. Working and counter electrodes were separated by a Whatman® glass microfiber filter. An A.C. signal of 10 mV was applied in the frequency range of 500 kHz to 10 mHz with 20 points per decade.

The determination of the electrochemical stability window and aluminum passivation tests were carried out using three electrode Swagelok® systems with lithium metal as reference electrode and polished platinum disks, or aluminum disks, (10 mm ø) as working and counter electrodes. The system was run for five cycles at 1 $mV.s^{-1}$ within the potential range of 0.01 V to 5 V for the determination of the electrochemical window and between 2 V and 4.7 V at 0.2 $mV.s^{-1}$ in the case of aluminum passivation tests.

The Scanning Electron Microscope (SEM) images where obtained using a Zeiss ultra + equipped with a secondary electron sensor.

The X-ray photoelectron spectroscopy (XPS) measurements were carried out with a Kratos Axis Ultra spectrometer, using a focused monochromatized Al Kα radiation (hν = 1486.6 eV). The XPS spectrometer was directly connected to an argon dry box, through a transfer chamber, to avoid moisture/air exposure of the samples. The spectrometer was calibrated using the photoemission line Ag $3d_{5/2}$ (binding energy 368.3 eV). For the Ag $3d_{5/2}$ line, the full width at half-maximum was 0.58 eV under the recording conditions. The analyzed area of the samples was 300 µm x 700 µm. The analyzing depth of the XPS experiment was the first 5 nm of the surface of the electrode. Peaks were recorded with a constant pass energy of 20 eV. The pressure in the analysis chamber was around 1 x 10^{-9} Pa. Short acquisition time spectra were recorded before and after each experiment and compared to make sure the

samples did not suffer from degradation under X-ray beam during measurements. The binding energy scale was calibrated from the hydrocarbon contamination using C1s peak at 285.0 eV. Core peaks were analyzed using a non-linear Shirley-type background [17]. The peak positions and areas were optimized by a weighted least squares fitting method, using 70 % Gaussian, 30 % Lorentzian lineshapes. Quantification of the chemical species at the surface was performed on the basis of Scofield's relative sensitivity factors [18]. The coin-cells were opened in the argon-filled glove box and the electrodes were rinsed there with DMC. The DMC rinse was used to remove electrolyte salt residues that are not inherent to the SEI. During rinsing, the electrode samples were soaked in 2 mL DMC for 30 min and then dried for 1 h (under reduced pressure) at ambient temperature. The electrode samples were then mounted on the XPS sample holder in the Ar glove box and sent to the IPREM laboratory under vacuum for XPS analysis. Baseline data for the anodes was achieved by analyzing a pristine sample.

3. Results and discussion

3.1. EGM as solvent mixture for a LiTDI based LiB electrolyte

The physical properties of the EGM mixture and each of its pure components [19, 20] are reported in table 1 together with those [21] of the EC/DMC mixture given for comparison.

Table 1.

GBL has been chosen as a component of the mixture for its high dipolar moment, its high permittivity and relatively low viscosity. Hence, lithium salts are readily dissolved in this solvent and their solutions exhibit high conductivity [22, 23]. Another interesting property is the large temperature domain in which it remains liquid. However, GBL cannot be used in commercial cells with $LiPF_6$ as lithium salt as it forms a highly resistive solid electrolyte interphase (SEI) on graphite which affects badly the battery performance [24]. EC was chosen

as a co-solvent mainly for its ability to form a stable SEI on graphite and also for its high polarity, high permittivity and high boiling point [25]. Finally, MP was chosen as a third co-solvent for its low viscosity and low melting temperature with the aim of increasing the fluidity of the electrolyte and reducing the solidification point of the mixture. As a result, the EGM mixture exhibits a lower viscosity than EC/DMC and a higher permittivity which favours salt dissociation.

In the presence of 1 mol.L^{-1} LiTDI the conductivities range from 4.33 mS.cm^{-1} (LiTDI-EC) to 8.32 mS.cm^{-1} (LiTDI-EGM). Only by mixing EC, GBL and MP together could the optimum conductivity be obtained meaning that the contribution of the ternary mixture to the electrolyte conductivity is greater than the contributions offered by each of its separate pure solvents.

3.1.1. Electrochemical and thermal stability

The electrochemical stability windows of electrolytes containing LiTDI at 1 mol.L^{-1} in EC/DMC or EGM have been investigated on a platinum electrode in the presence of 2 % by weight of FEC. The latter is added as a SEI forming additive. Cyclic voltammograms presented in figure 1 show that the anodic limit of these electrolytes is limited to 4.7 V vs. Li^+/Li owing to the oxidation of TDI^- anions [7]. Indeed, it has been reported that the solvent mixture itself is stable up to at least 5 V [26]. It was also noticed that the use of EGM increased the potential at which the anion oxidation starts.

Figure 1.

The reduction peaks situated at 1.9 V vs. Li^+/Li is attributed to water as the mean water content of LiTDI solutions are around 100 ppm. The following peaks at 1.5 V vs. Li^+/Li and 0.8 V vs. Li^+/Li correspond to the reduction of the SEI forming compounds: FEC and EC respectively.

The thermal stability of LiTDI in EC/DMC and in EGM was investigated through DSC experiments. The DSC traces of the EGM and EC/DMC based electrolytes, obtained at 2 °C.min^{-1}, are reported in figure 2. Both electrolytes can withstand temperatures up to ≈ 130 °C, LiTDI-EGM being more stable owing to the lower amount of volatile solvents such as MP and DMC (T_b < 100 °C) in the mixture. As expected, the LiTDI-EGM electrolyte undergoes no phase change between -60 °C and 130 °C whereas LiTDI-EC/DMC solidifies at -40 °C and presents, on the reverse scan, a characteristic eutectic peak followed by the fusion of the remaining crystals. No solidification peak is observed in the case of LiTDI-EGM suggesting a stability of this electrolyte at even lower temperatures.

Figure 2.

3.1.2. Conductivity and ion-pair dissociation of LiTDI in EGM

Taking into account the thermal stability of LiTDI-EGM, the conductivity of this electrolyte was measured from -40 °C to 80 °C. Conductivity values are presented in figure 3 as a function of the salt concentration at several temperatures.

Figure 3.

The electrolyte conductivity increases with LiTDI concentration due to an increasing number of charged species before reaching a maximum that depends on the temperature (this phenomenon is the consequence of the increase in fluidity when the temperature is raised).

At higher salt concentrations, the electrolyte viscosity increase becomes predominant and as a result, the conductivity decreases. It should also be noted that the increasing salt concentration favors the formation of ion-pairs (IPs) and larger aggregates that also contribute to the drop in conductivity. From literature data, the conductivities of electrolytes containing LiTDI at 1 mol.L^{-1} can be compared: EGM allows the highest conductivity with 8.5 mS.cm^{-1} at 25 °C,

followed by EC/DMC with 6.8 $mS.cm^{-1}$ at 25 °C [10], 8EC/16DMC/1DME (dimethoxyethane) with 6.13 $mS.cm^{-1}$ at 25 °C [12], and finally 3EC/7DEC(diethyl carbonate) with 3.39 $mS.cm^{-1}$ at 20 °C [8].

LiTDI-EGM also exhibits a relatively high conductivity at low temperature (1.65 $mS.cm^{-1}$ at -40 °C) making it a good candidate for low temperature applications. In comparison, $LiPF_6$ in EC/DEC/DMC/MA (methyl acetate) has a conductivity of 2 $mS.cm^{-1}$ at -40 °C [27].

Figure 4.

The dissociation coefficient (α_D) of LiTDI in EGM and EC/DMC was calculated using the Walden rule [10, 28, 29], as reported in the experimental section, and values are plotted as a function of the temperature and LiTDI concentration in figures 4a and 4b. It is interesting to notice that the dissociation coefficient of LiTDI does not depend on the temperature. This is due to a coupling effect between the conductivity and viscosity of LiTDI [10, 13]. The dissociation coefficient of LiTDI is larger in EGM (37 %) than in EC/DMC (31 %) and is not temperature dependent. As seen in figure 4b, α_D decreases sharply when the salt concentration is increased.

3.2. Passivation layers at interfaces

The ability of an electrolyte to prevent cathodic current collector corrosion or anodic graphite exfoliation by forming a stable passivation layer is essential to the cell life-span and its capacity retention.

3.2.1. Aluminum passivation

It has already been demonstrated that LiTDI in EC/DMC and EC/DEC does not continuously corrode aluminum [7, 8]. The cyclic voltammograms (CV) presented in figure 5 prove that, as expected, LiTDI-EGM also does not continuously corrode aluminum. Corrosion

can be observed on the first CV cycle at 3.8 V *vs.* Li^+/Li but stops as of the second CV cycle. The inset x 500 SEM image in figure 5 represents the surface of an aluminum current collector after 20 cycles in the presence of LiTDI-EGM. The EDX analysis, not presented here, reveals the existence of Al and O elements only.

Figure 5.

Until now it was not known if LiTDI participated in the formation of a passivating layer as $LiPF_6$ does by forming a AlF_3 film on top of the aluminum oxide layer [30], or if it left the native aluminum oxide (Al_2O_3) layer intact. A XPS survey spectrum (not presented here) revealed the presence of the following elements at the surface of an aluminum electrode cycled in the presence of LiTDI-EGM+2%FEC: fluoride (F1s), oxygen, nitrogen (N1s), carbon (C1s) and aluminum (Al2p). Al2p, C1s, F1s and N1s XPS spectra are presented in figure 6.

Figure 6.

The Al2p spectrum shows a presence of metallic aluminum (71 – 72 eV) and of an oxide or hydroxide layer (73 – 76 eV) which proves that LiTDI does not attack the oxide-hydroxide layer even after 20 cycles to form AlF_3. It can also be noted that no partially fluorinated Al compounds are detected at a higher binding energy (76 eV). The F1s spectrum exhibits two contributions: the first one (F1) at 685 eV is assigned the presence of LiF formed by the decomposition of the FEC additive and possibly that of LiTDI also. The second contribution (F2) at 688 eV represents a different chemical environment corresponding to fluorinated aluminum. As the intensity of this peak was found to be very low, it is possible that it corresponds to a light fluorination of the aluminum plate which was not detected on the Al2p spectrum due to the strong signal of the $Al_2O_3/Al(OH)_3$ surface oxide. According to the C1s

spectrum there are no traces of carbonates at 290 eV and, also, no CF_3 groups at 293 eV coming from the TDI^- anion. Two peaks can be observed on the N1s spectrum at 399 eV (N2) corresponding to the LiTDI cyanide functions (C≡N) and at 402–403 eV (N3) which corresponds well to an azide or -(N^-)- specie (402.1 eV) [31]. In conclusion, the F1s spectrum suggests that, like $LiPF_6$, LiTDI helps form a AlF_3 protective layer at the surface of the aluminum electrode.

3.2.2. Solid Electrolyte Interface

EIS study

The electrochemical impedance diagram of a lithiated graphite electrode dipped in the LiTDI-EGM+2%FEC electrolyte is displayed in figure 7 as a Nyquist plot.

Figure 7.

The high frequency half-circle represents the SEI resistance (R_{SEI}) and its intersection with the X-axis is the electrolyte resistance (R_{el}). The second half-cycle (at medium frequencies) corresponds to the charge transfer resistance (R_{ct}). Values of R_{el}, R_{SEI} and R_{ct} resistances, obtained by fitting the Nyquist plots, are plotted as a function of the Gr/Li half-cell cycle number in figure 8 along with those obtained using LiTDI and $LiPF_6$ in EC/DMC as electrolytes.

It can be noticed that all electrolytes follow a similar pattern. As expected R_{el} does not vary significantly with the cycle number. Variations of R_{ct} are limited to a dozen ohms (around 14 Ω for $LiPF_6$-EC/DMC+2%FEC and LiTDI-EGM+2%FEC and 20 Ω for LiTDI-EC/DMC+2%FEC). R_{SEI} increases until it reaches a horizontal asymptote at the 15^{th} cycle: $R_{SEI,limit}$ = 9.5 Ω for the $LiPF_6$-based electrolyte and respectively 12.5 Ω and 15 Ω for LiTDI-EGM+2%FEC and LiTDI-EC/DMC+2%FEC.

Figure 8.

The necessity of an SEI forming additive such as FEC is demonstrated in figure 9 where are reported the capacity variations of the graphite electrode in LiTDI-EC/DMC and $LiPF_6$-EC/DMC electrolytes, both additive-free, as a function of the cycling rate (discharge rates from D/24 to D/5).

Figure 9.

Without the use of a SEI forming additive, the capacity of the graphite electrode drops at about 50 % of the initial capacity when the discharge rate is increased from D/24 to D/5 in the presence of the LiTDI based electrolyte whereas the loss in capacity is only of 16 % with the $LiPF_6$ based electrolyte. LiTDI is responsible for the formation of a more resistive SEI which limits the migration of Li^+ cations when the discharge rate is increased. As suggested by Shkrob *et al.* [32], in the absence of SEI forming additives LiTDI undergoes a peculiar decomposition leading to radicals that disfavor radical polymerization of the solvent over its anionic polymerization and, as a result, leads to the formation of a high resistance SEI.

XPS analysis and SEM observation

The F1s, C1s and N1s XPS spectra of the graphite surface cycled in LiTDI-EGM+2%FEC are displayed in figure 10 along with a SEM image showing the delithiated graphite electrode surface after two C/24 cycles. A granular layer corresponding to the extreme surface of the SEI covers the surface.

Figure 10.

A higher LiF concentration (18.0 % LiF) was found at the surface of the graphite electrode cycled in LiTDI-EGM+2%FEC against only 5.5 % in LiTDI-EC/DMC+2%FEC. This

increase in LiF concentration is due to the decomposition of FEC and of TDI^- anions which follows a different mechanism when EC/DMC is replaced by EGM. The increase in mineral compounds like LiF over organic species (lithium alkylcarbonates and polymers) thus results in a less resistive SEI. The F2 region in the same F1s spectrum corresponds to CF_3 groups originating from the TDI^- anion.

In the C1s spectrum, the CF_3 peak is almost undetectable as compared to the peaks belonging to carbon species such as carbonates (C4) meaning that LiTDI is a minor compound at the surface of the electrode. Carbonates represent respectively 49 % and 43 % of the graphite surface after cycling in LiTDI-EC/DMC+2%FEC and LiTDI-EGM+2%FEC. The C1, C2 and C3 regions correspond respectively to the C-C, C-OH and C=O chemical bonds.

The N1s spectrum presents two different nitrogen regions. The N1 (398 eV) and N2 (399-400 eV) regions correspond respectively to nitride ions (N^{3-} as in Li_3N) and to cyanide groups belonging to LiTDI. As TDI^- anions are the sole source of nitrogen, the presence of lithium nitride suggests a possible reductive decomposition of TDI^-.

3.3. Galvanostatic cycling performance

In this section, the electrolytes LiTDI-EGM+2%FEC (El-1), LiTDI-EC/DMC+2%FEC (El-2) and $LiPF_6$-EC/DMC+2%FEC (El-3) were tested in NMC/Li and Gr/Li half-cells and in a NMC/Gr full cell at room temperature. As the LiTDI-EGM electrolyte has a sufficient conductivity at -20 °C (2.8 $mS.cm^{-1}$), it was possible to test this electrolyte in the full cell configuration at -20 °C. Moreover, as the LiTDI-EGM mixture is thermally stable until at least 130 °C, unlike the $LiPF_6$-based electrolyte which starts releasing HF and PF_5 [8], experiments were also performed at 60 °C using the EL-1 electrolyte in the full cell configuration. Finally, extended cycling of NMC/Gr cells was performed.

3.3.1. Irreversible capacity

The percentage of the irreversible capacities (IR) was calculated according to the following equation:

$$IR_{n+1} = \frac{100(Q_{C.n} - Q_{C.n+1})}{Q_{C.i}} \quad \text{Eq. 4}$$

where $Q_{C.i}$ is the initial charge capacity and $Q_{C.n}$ is the charge capacity at cycle n. Results are reported in table 2.

For the LiTDI based electrolytes similar results were obtained in EGM and in EC/DMC. Gr/Li half-cells irreversible capacities are negligible as of the 4th cycle and the coulombic efficiency reaches 99.99 %. For $LiPF_6$ one more cycle is needed to reach these values. In NMC/Li half-cells the IR are higher and stabilization occurs only at the 5th cycle. The IR in NMC/Gr cells are close to those of the NMC/Li half cells and also become negligible after 5 cycles. In all cases, the $LiPF_6$ based electrolyte leads to higher irreversible capacities.

Table 2.

3.3.2. Power capability in half-cells

The discharge capacities of graphite and NMC electrodes were measured in half-cells at several discharge rates, the charge rate being kept constant at C/5 as of the 5th cycle. In figure 11 are reported the graphite and NMC charge/discharge voltage profiles (a and b) using El-1 electrolyte along with the discharge capacities obtained for each electrolyte under increasing discharge rate (c and d).

El-1 and El-2 electrolytes exhibit similar performances in Gr/Li half-cells up to 6D with capacity retentions respectively equal to 92.5 % and 87.6 %. El-3 could not be used in Gr/Li half-cells at discharge rates over 2D.

El-1 displays better performances than El-2 or even El-3 in NMC/Li half-cells up to 6D with capacity retentions of respectively 66.7 %, 56.8 % and 64.4 %. The higher specific capacities obtained in NMC/Li and Gr/Li half-cells using El-1 are due to a combination of many factors such as the electrolyte conductivity, the interfacial resistances, the salt dissociation and lithium solvation.

Figure 11.

3.3.3. Power capability of NMC/Gr full-cells

In NMC/Gr full cells, the limiting electrode is the NMC in order to avoid any lithium plating of the negative electrode. Hence, the reported discharge capacities are those of the NMC electrode, the charging rate being kept constant at C/5 from the 5th cycle to the last. The cell voltage profile obtained using the El-1 electrolyte is displayed in figure 12 along with the NMC capacities using all three electrolytes as a function of the cycle number.

Figure 12.

The El-1, El-2 and El-3 electrolytes exhibit similar performances up to 7D with respectively 51.5 %, 53.8 % and 60.0 % capacity retention. At discharge rates over 7D, the cells using LiTDI-based electrolytes undergo a more important drop in capacity than those using $LiPF_6$. The better capacity retention observed in the case of the $LiPF_6$-based electrolyte at high discharge rate is likely the consequence of a lower battery internal resistance. Indeed, El-3 has a higher conductivity, which contributes to a lower internal resistance, as well as lower interfacial resistances than the LiTDI-based electrolytes. At a 10D rate only 38.5%, 26.9% and 52.0% of the initial capacity is recovered respectively with El-1, El-2 and El-3. Both LiTDI-based electrolytes present similar behavior even if El-1 leads to better capacities up to 4D but not at higher rates. As a conclusion, LiTDI is a very promising lithium salt for LiB as

it could sustain up to 7D discharge rates with more than 50 % capacity retention in NMC/Gr cells.

In the following two sections we investigate how NMC/Gr cells containing LiTDI are affected by low (-20 °C) and high (60 °C) functioning temperatures and compare the more thermally stable El-1 to El-2.

3.3.4. Power capability in NMC/Gr cells at low temperature (-20 °C)

In order to study the impact of low temperatures on the capacities of NMC/Gr cells using the LiTDI based El-1 and El-2 electrolytes, two different tests were carried out. In the first test, the SEI formation was done at room temperature and the cell was afterwards discharged (charged) at -20 °C at D/24 (C/24) for 3 cycles, D/5 (C/5) for 5 cycles and D (C/5) for 20 cycles (Fig. 13.a). The second test was similar but the SEI formation and cycling were both done at -20 °C (Fig. 13.b)

Figure 13.

According to the results presented in figure 13, the temperature at which is formed the SEI has only a limited impact on the cycling capacities measured at -20 °C. However, the latter are lower than those obtained at room temperature and the gap between the two increases with the charge/discharge rate. At C rate, only 31 % of the capacity measured at room temperature is obtained at -20 °C. Still, it can be noticed that the EGM solvent mixture allows better results than EC/DMC. For each test, the coulombic efficiency was found to be close to 100 %. The charge/discharge profiles of NMC/Gr cells cycled at -20 °C (Fig. 14.a) and at room temperature (Fig. 14.b) are reported Figure 14. At -20 °C, the charge capacity at the first cycle is always higher than those of the following cycles. This phenomenon does not occurs at room temperature and means that part of the lithium inserted in the graphite electrode remains

trapped between the layers owing to a low kinetic. The positive NMC electrode is likely responsible for this phenomenon as this material is less electron-conducting at low temperatures [33] inducing an ohmic voltage drop.

Figure 14.

When the cell temperature is set back to room temperature after cycling at -20 °C, full capacity recovery is achieved for the El-1 electrolyte with a coulombic efficiency of 99.9 % and for El-2, a value close to the full capacity is obtained (Figure 15). Hence, the capacity loss observed at -20 °C when the charge/discharge rate is increased is reversible.

Figure 15.

3.3.5. Power capability in NMC/Gr cells at high temperature (60 °C)

Similar power capability tests were carried out at 60 °C. Because of the increase in electrolyte fluidity and conductivity and decrease in the internal resistance of the cells, higher capacities and coulombic efficiencies are expected. However, as presented in figure 15, a decrease in NMC/Gr cell capacity is observed at 60 °C. Moreover, even if the SEI layer is formed at room temperature instead of 60 °C, only a little increase in the discharge capacities is noted. This means also that the SEI is not responsible for the lower capacities measured at 60 °C as compared to room temperature. It was also noticed that instead of being close to 100 %, the coulombic efficiency is less than 99 %: 90 % at a C/5 rate and 95 % at a C rate in both electrolytes. This means that parasitic reactions occur at the surface of the electrodes like solvent oxidation at the positive electrode or/and SEI dissolution at the negative electrode.

Figure 16.

When the temperature is set back to room temperature, the discharge capacities stayed unchanged as indicated by the graph reported in Figure 16, proving that the capacity loss observed at 60 °C is irreversible.

Figure 17.

The observed capacity loss at 60°C could be related to the decomposition of EC as reported by Kerner *et al* [34]. At 70°C, the authors found that EC, in the presence of LiTDI, underwent a decomposition process leading to the production of CO_2 as it does when in the presence of thermal decomposition products of PF_6^- [14].

3.3.6. Durability tests in NMC/Gr full-cell configuration

Extended cycling was performed at room temperature using the Gr/NMC cell with LiTDI-based electrolytes (El-1 and El-2) and $LiPF_6$-based electrolyte (El-3). The evolution of the discharge capacity with the cycle number is displayed in figure 17. The charge/discharge rate was set at 1C/1D after forming the SEI at C/24 (one cycle only).

Figure 18.

According to the graphs presented in figure 17, both LiTDI-based electrolytes permitted higher discharge capacities than the $LiPF_6$-based electrolyte. The LiTDI-EGM+2%FEC electrolyte leads to the best results as 850 cycles could be performed before the cell lost 30 % of its initial capacity.

Conclusion

A new electrolyte using the LiTDI lithium salt has been formulated. The solvent used is a ternary EC/GBL/MP mixture which allows a better dissociation of the lithium salt than the

classical EC/DMC binary mixture. The LiTDI-EGM electrolyte is capable of withstanding temperatures going from -60 °C to 130 °C without undergoing phase transitions. Its conductivity is higher than 1 $mS.cm^{-1}$ at -40 °C making it an interesting electrolyte for low temperature applications. This electrolyte formulation is stable up to 4.7 V vs. Li^+/Li, does not corrode aluminum and allows the formation of a stable SEI on graphite in the presence of FEC. In terms of power capability, it is able to withstand high discharge rates (up to 7D) in full NMC/graphite cells. LiTDI-EGM, also being more fluid and conductive than LiTDI-EC/DMC, allows better capacities at low temperatures (-20 °C). However, at high temperature (≥ 60 °C), an irreversible capacity loss occurs for full Gr/NMC cells. EC is suspected to decompose in the presence of LiTDI at 60 °C or more. Extended cycling of a Gr/NMC cell containing the LiTDI-EGM electrolyte show that 850 cycles could be performed before losing 30 % of the initial capacity.

References

1. Erickson, E.M., C. Ghanty, and D. Aurbach, *New Horizons for Conventional Lithium Ion Battery Technology.* The Journal of Physical Chemistry Letters, 2014. **5**(19): p. 3313-3324.
2. Duncan, H., N. Salem, and Y. Abu-Lebdeh, *Electrolyte Formulations Based on Dinitrile Solvents for High Voltage Li-Ion Batteries.* Journal of The Electrochemical Society, 2013. **160**(6): p. A838-A848.
3. Eshetu, G.G., et al., *LiFSI vs. LiPF6 electrolytes in contact with lithiated graphite: Comparing thermal stabilities and identification of specific SEI-reinforcing additives.* Electrochimica Acta, 2013. **102**(0): p. 133-141.
4. Niedzicki, L., et al., *New type of imidazole based salts designed specifically for lithium ion batteries.* Electrochimica Acta, 2010. **55**(4): p. 1450-1454.
5. Gnanaraj, J.S., et al., *LiPF3(CF2CF3)(3): A salt for rechargeable lithium ion batteries.* Journal of The Electrochemical Society, 2003. **150**(4): p. A445-A454.
6. Dahbi, M., et al., *Comparative study of EC/DMC LiTFSI and LiPF6 electrolytes for electrochemical storage.* Journal of Power Sources, 2011. **196**(22): p. 9743-9750.
7. Niedzicki, L., et al., *New covalent salts of the 4V class for Li batteries.* Journal of Power Sources, 2011. **196**(20): p. 8696-8700.
8. Paillet, S., et al., *Power capability of LiTDI-based electrolytes for lithium-ion batteries.* Journal of Power Sources, 2015. **294**: p. 507-515.
9. Paillet, S., et al., *Determination of the electrochemical performance and stability of the lithium-salt, lithium 4,5-dicyano-2-(trifluoromethyl) imidazolide, with various anodes in Li-ion cells.* Journal of Power Sources, 2015. **299**: p. 309-314.
10. Berhaut, C.L., et al., *LiTDI as electrolyte salt for Li-ion batteries: transport properties in EC/DMC.* Electrochimica Acta, 2015. **180**: p. 778-787.
11. Niedzicki, L., B. Brzozowski, and P. Wieczorek, *LiTDI and solvent mixture based electrolytes for lithium-ion cells.* Electrochimica Acta, 2015. **174**: p. 625-629.
12. Niedzicki, L., et al., *Optimization of the lithium-ion cell electrolyte composition through the use of the LiTDI salt.* Electrochimica Acta, 2014. **117**(0): p. 224-229.
13. Berhaut, C.L., et al., *Ionic association analysis of LiTDI, LiFSI and LiPF6 in EC/DMC for better Li-ion battery performances.* RSC Advances, 2019. **9**(8): p. 4599-4608.
14. Sloop, S.E., et al., *Chemical Reactivity of PF_5 and LiPF6 in Ethylene Carbonate/Dimethyl Carbonate Solutions.* Electrochemical and Solid-State Letters, 2001. **4**(4): p. A42-A44.
15. Sun, X., et al., *Using a Boron-Based Anion Receptor Additive to Improve the Thermal Stability of LiPF6-Based Electrolyte for Lithium Batteries.* Electrochemical and Solid-State Letters, 2002. **5**(11): p. A248-A251.
16. Markevich, E., et al., *Reasons for capacity fading of LiCoPO4 cathodes in LiPF6 containing electrolyte solutions.* Electrochemistry Communications, 2012. **15**(1): p. 22-25.
17. Shirley, D.A., *High-Resolution X-Ray Photoemission Spectrum of the Valence Bands of Gold.* Physical Review B, 1972. **5**(12): p. 4709-4714.
18. Scofield, J.H., *Hartree-Slater subshell photoionization cross-sections at 1254 and 1487 eV.* Journal of Electron Spectroscopy and Related Phenomena, 1976. **8**(2): p. 129-137.
19. Marcus, Y., *Ion solvation*. 1985: Wiley.

20. Welton, C.R.a.T., *Solvents and Solvent Effects in Organic Chemistry*. 4th edition ed. 2011: Wiley-VCH. 718.
21. Rodríguez, A., et al., *Viscosities of Dimethyl Carbonate or Diethyl Carbonate with Alkanes at Four Temperatures. New UNIFAC−VISCO Parameters.* Journal of Chemical & Engineering Data, 2003. **48**(1): p. 146-151.
22. Huang, J.-y., et al., *Study on γ-butyrolactone for LiBOB-based electrolytes.* Journal of Power Sources, 2009. **189**(1): p. 458-461.
23. Xu, K., *Nonaqueous Liquid Electrolytes for Lithium-Based Rechargeable Batteries.* Chemical Review, 2004. **104**: p. 4303-4417.
24. Kinoshita, S.-c., et al., *Effects of cyclic carbonates as additives to γ-butyrolactone electrolytes for rechargeable lithium cells.* Journal of Power Sources, 2008. **183**(2): p. 755-760.
25. Fong, R., U. von Sacken, and J.R. Dahn, *Studies of Lithium Intercalation into Carbons Using Nonaqueous Electrochemical Cells.* Journal of The Electrochemical Society, 1990. **137**(7): p. 2009-2013.
26. Tarascon, J.M. and D. Guyomard, *New electrolyte compositions stable over the 0 to 5 V voltage range and compatible with the Li1+xMn2O4/carbon Li-ion cells.* Solid State Ionics, 1994. **69**(3): p. 293-305.
27. Smart, M.C., B.V. Ratnakumar, and S. Surampudi, *Development of High Conductivity Lithium-ion Electrolytes for Low Temperature Cell Applications*, 1998, Jet Propulsion Lab.: California Inst. of Tech., Pasadena, CA United States.
28. Schreiner, C., et al., *Fractional Walden Rule for Ionic Liquids: Examples from Recent Measurements and a Critique of the So-Called Ideal KCl Line for the Walden Plot†.* Journal of Chemical & Engineering Data, 2009. **55**(5): p. 1784-1788.
29. Longinotti, M.P. and H.R. Corti, *Fractional Walden Rule for Electrolytes in Supercooled Disaccharide Aqueous Solutions.* The Journal of Physical Chemistry B, 2009. **113**(16): p. 5500-5507.
30. Zhang, X. and T.M. Devine, *Factors That Influence Formation of AlF3 Passive Film on Aluminum in Li-Ion Battery Electrolytes with LiPF6.* Journal of The Electrochemical Society, 2006. **153**(9): p. B375-B383.
31. Zorn, G., et al., *X-ray Photoelectron Spectroscopy Investigation of the Nitrogen Species in Photoactive Perfluorophenylazide-Modified Surfaces.* The Journal of Physical Chemistry C, 2014. **118**(1): p. 376-383.
32. Shkrob, I.A., et al., *Chemical Stability of Lithium 2-Trifluoromethyl-4,5-dicyanoimidazolide, an Electrolyte Salt for Li-Ion Cells.* The Journal of Physical Chemistry C, 2016. **120**(50): p. 28463-28471.
33. Amin, R. and Y.-M. Chiang, *Characterization of Electronic and Ionic Transport in Li1-xNi0.33Mn0.33Co0.33O2 (NMC333) and Li1-xNi0.50Mn0.20Co0.30O2 (NMC523) as a Function of Li Content.* Journal of The Electrochemical Society, 2016. **163**(8): p. A1512-A1517.
34. Kerner, M., et al., *Towards more thermally stable Li-ion battery electrolytes with salts and solvents sharing nitrile functionality.* Journal of Power Sources, 2016. **332**: p. 204-212.

Figures

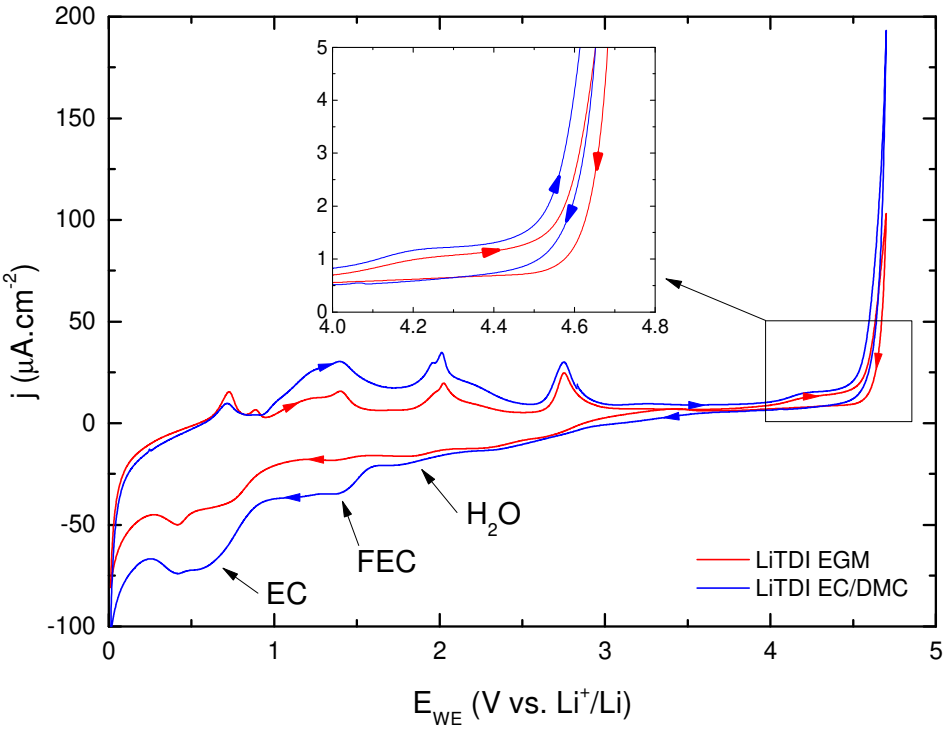

Figure 1. Cyclic voltammograms at 1 $mV.s^{-1}$ of LiTDI (1 $mol.L^{-1}$) in EGM+2%FEC and in EC/DMC+2%FEC at a Pt electrode. Reference and counter electrodes are respectively Li and Pt.

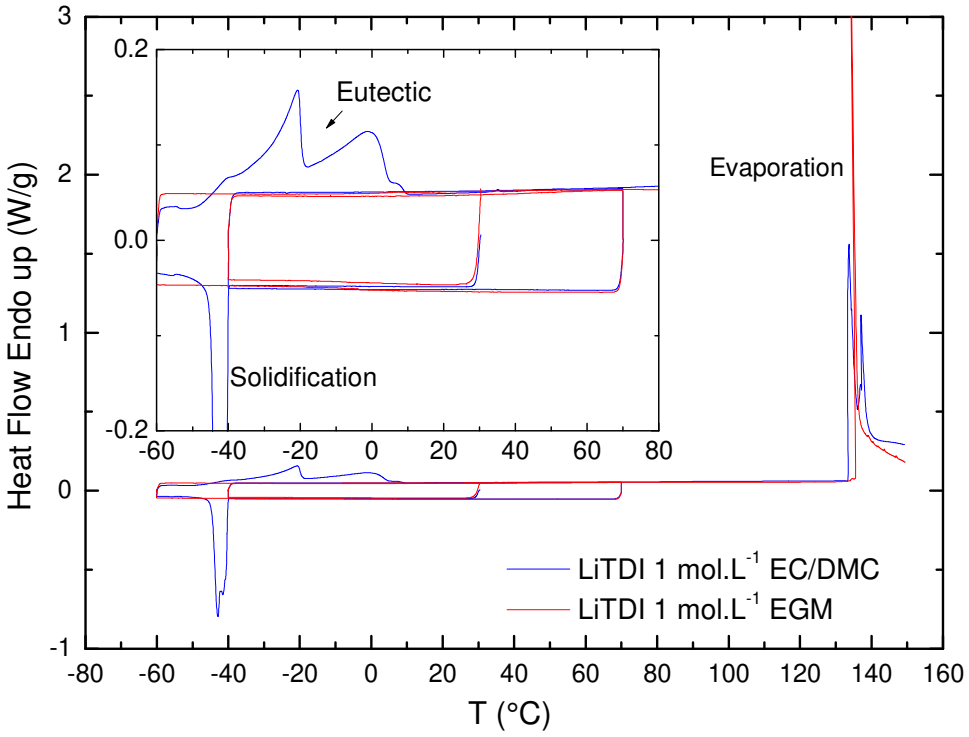

Figure 2. DSC traces of EGM and EC/DMC based electrolytes obtained at 2 °C.min^{-1} scan rate.

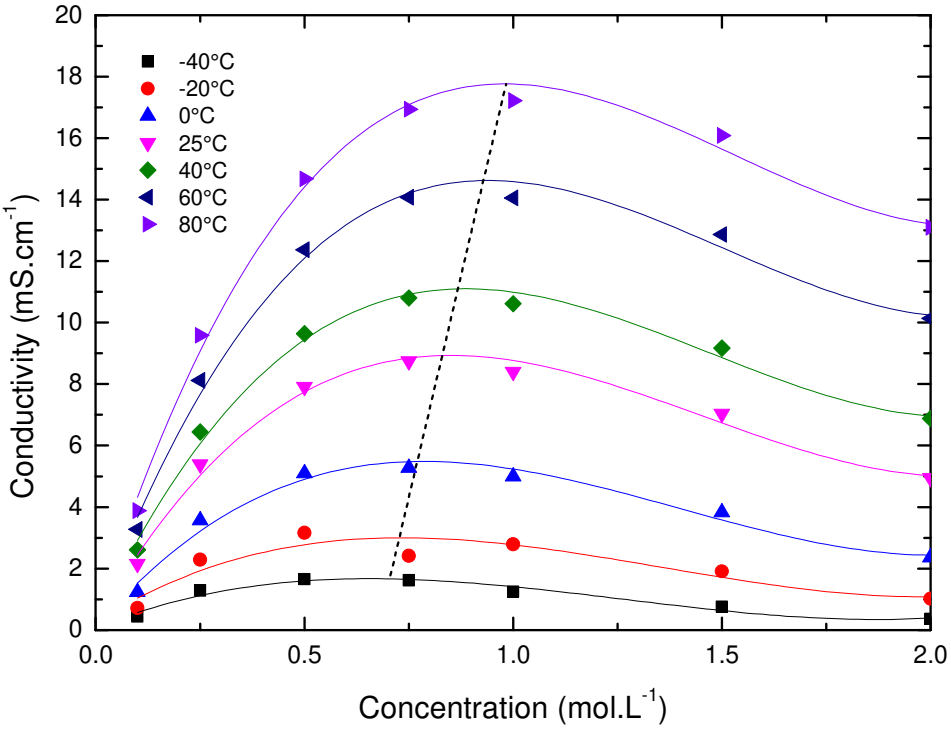

Figure 3. Conductivity of LiTDI in EGM as a function of the salt concentration and temperature.

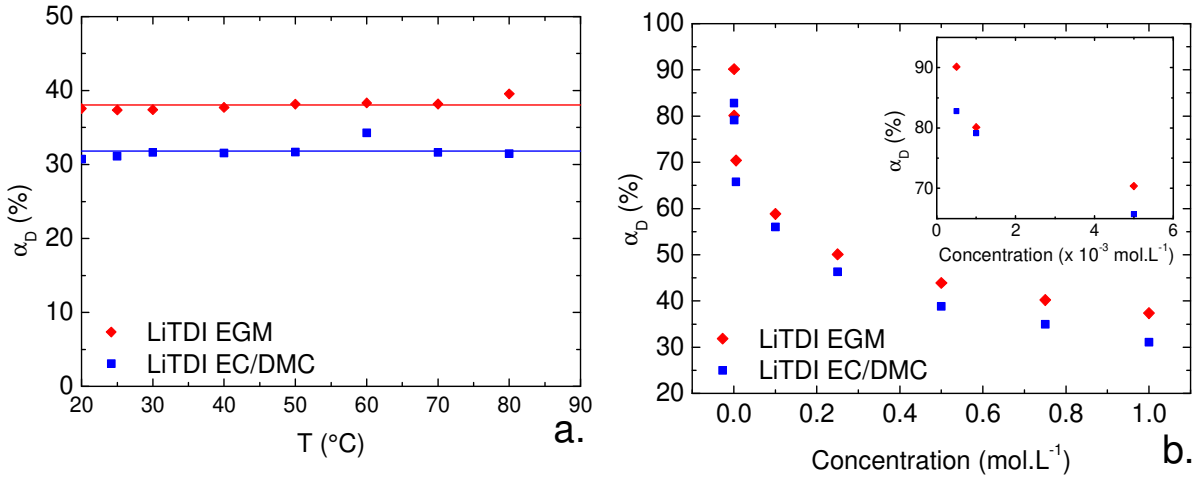

Figure 4. LiTDI dissociation coefficient in EC/DMC and EGM measured using the Walden rule as a function of (a) the temperature at 1 mol.L^{-1}, and (b) the salt concentration at 25 °C.

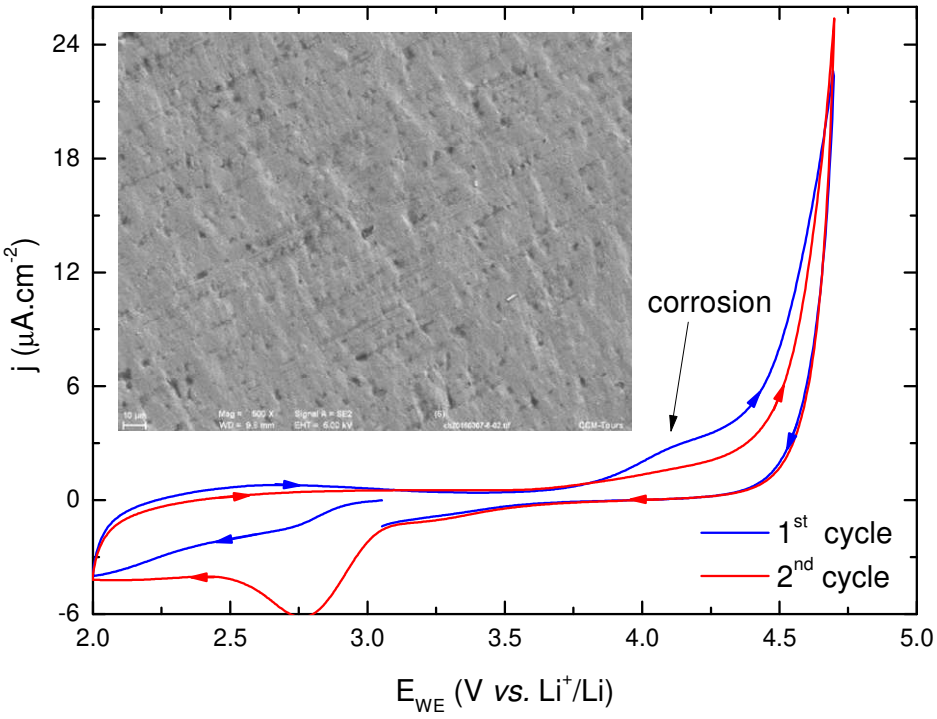

Figure 5. First and second voltammograms of an aluminum electrode in LiTDI-EGM between 2 V and 4.7 V at a 0.2 $mV.s^{-1}$ scan rate. The first CV started with an open circuit potential of 3.1 V. Inset is a SEM (x 500) image of the surface of the aluminum current collector after 20 cycles in LiTDI-EGM.

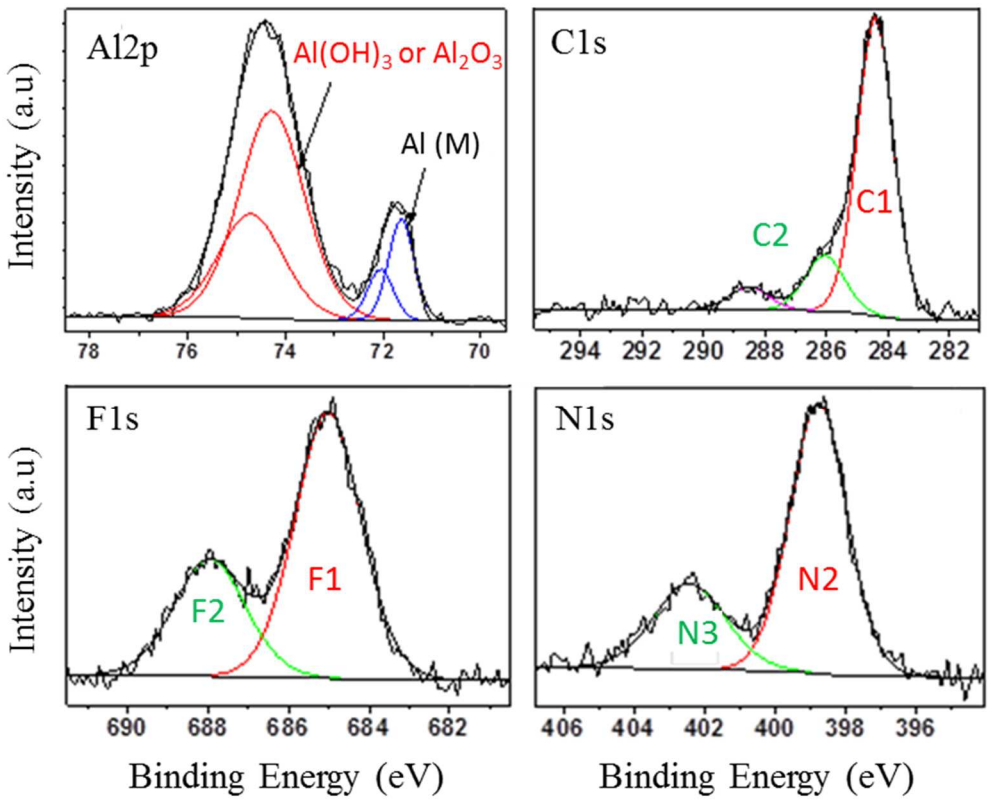

Figure 6. XPS spectra of the surface of an aluminum electrode after 20 CV cycles in the presence of the LiTDI-EGM+2%FEC electrolyte.

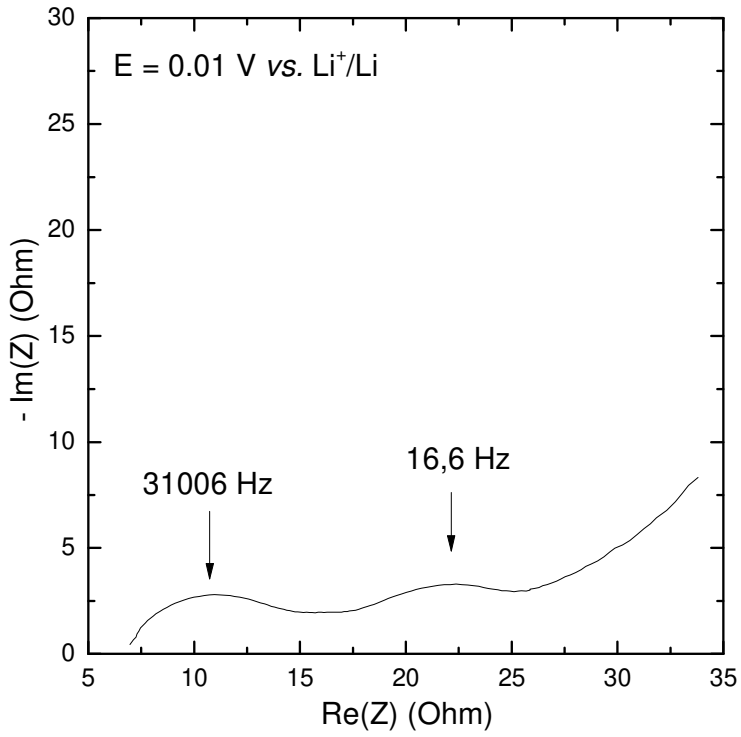

Figure 7. Nyquist plot of a lithiated graphite electrode dipped in LiTDI-EGM+2%FEC.

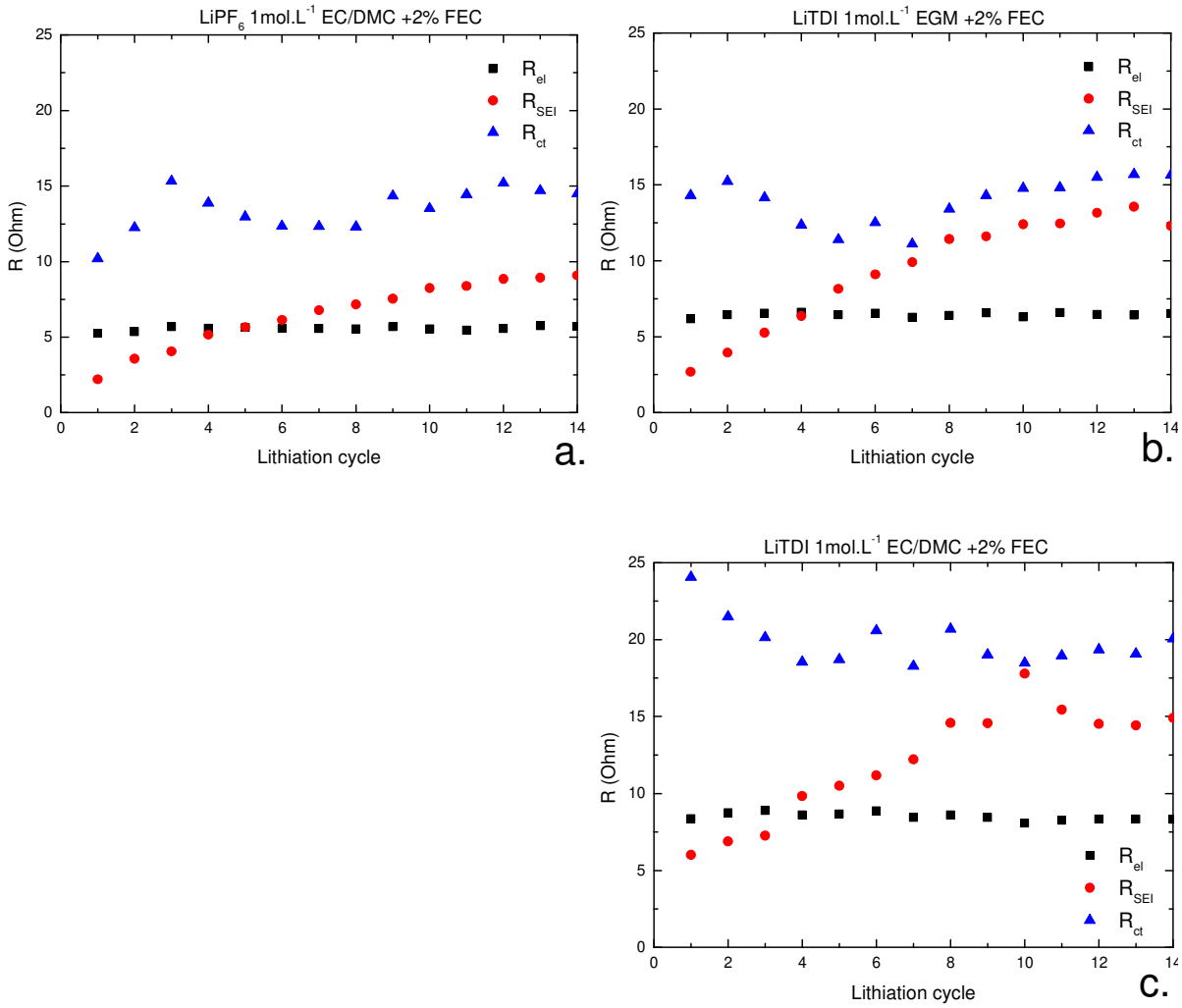

Figure 8. Variations R_{el}, R_{SEI} and R_{ct} of a graphite electrode dipped in (a) $LiPF_6$-EC/DMC+2%FEC, (b) LiTDI-EGM+2%FEC, and (c) LiTDI-EC/DMC+2%FEC. The graphite electrode was cycled at a C/10 rate in a Gr/Li half-cell configuration between 0.01 V and 1 V.

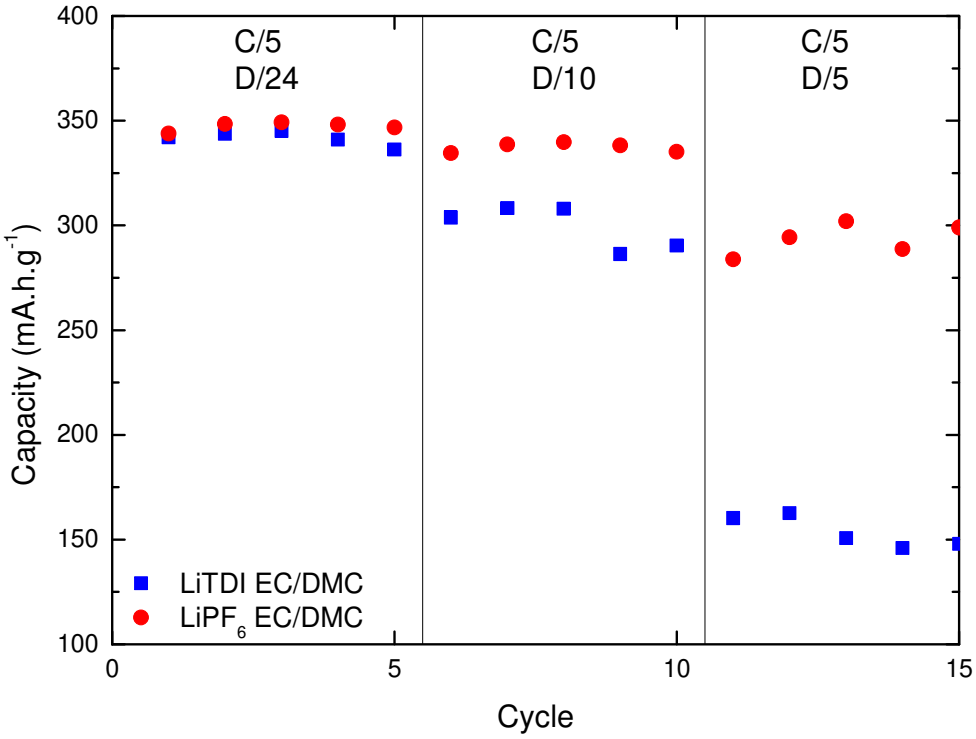

Figure 9. Discharge capacities of a graphite electrode cycled in a Gr/Li half-cell using LiTDI-EC/DMC or $LiPF_6$-EC/DMC at a C/5 charge rate and D/24 to D/5 discharge rates.

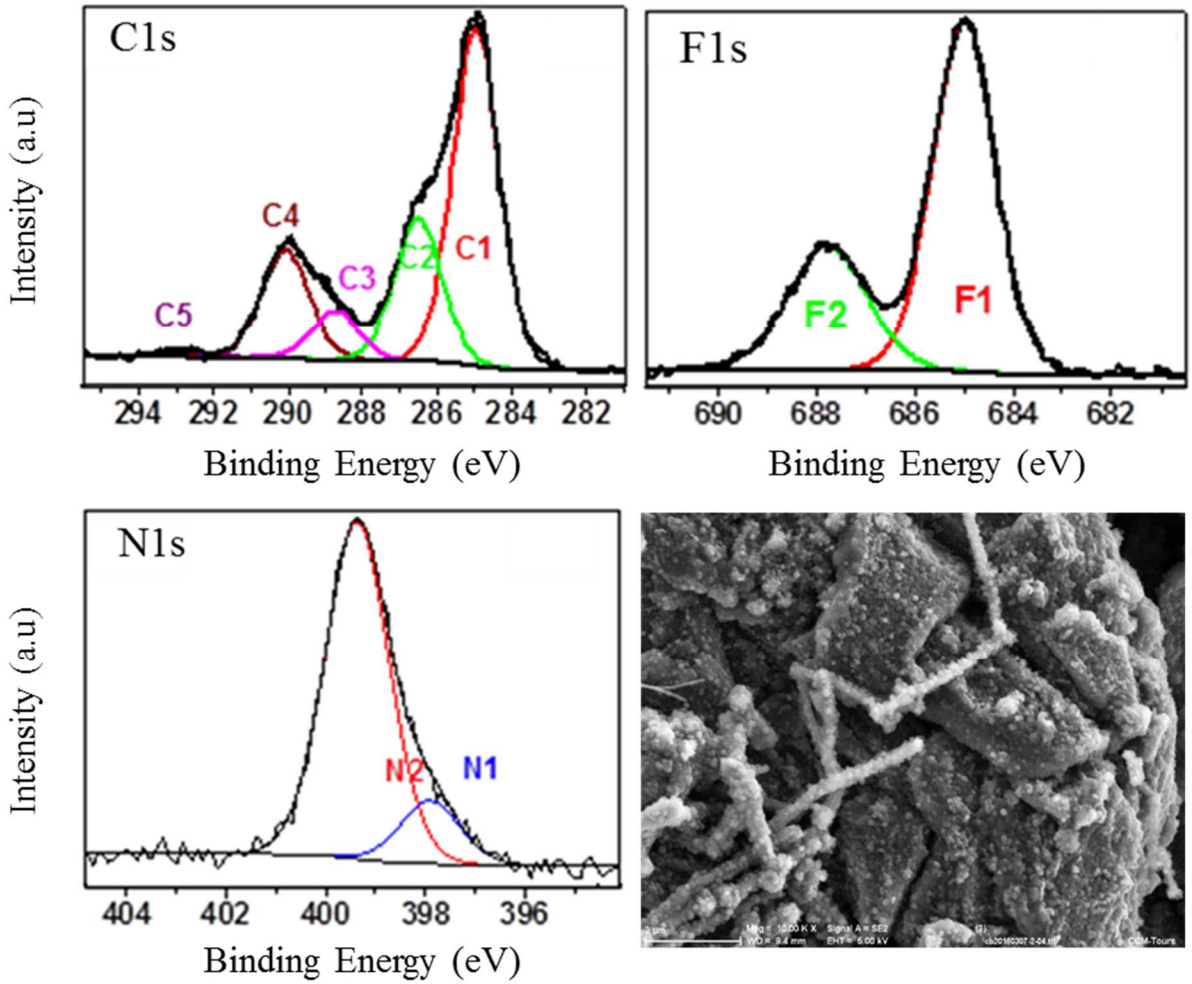

Figure 10. XPS spectra of the elemental composition of the surface of a delithiated graphite electrode after two cycles at C/24 in the presence of LiTDI-EGM+2%FEC and x 10000 SEM image of its surface.

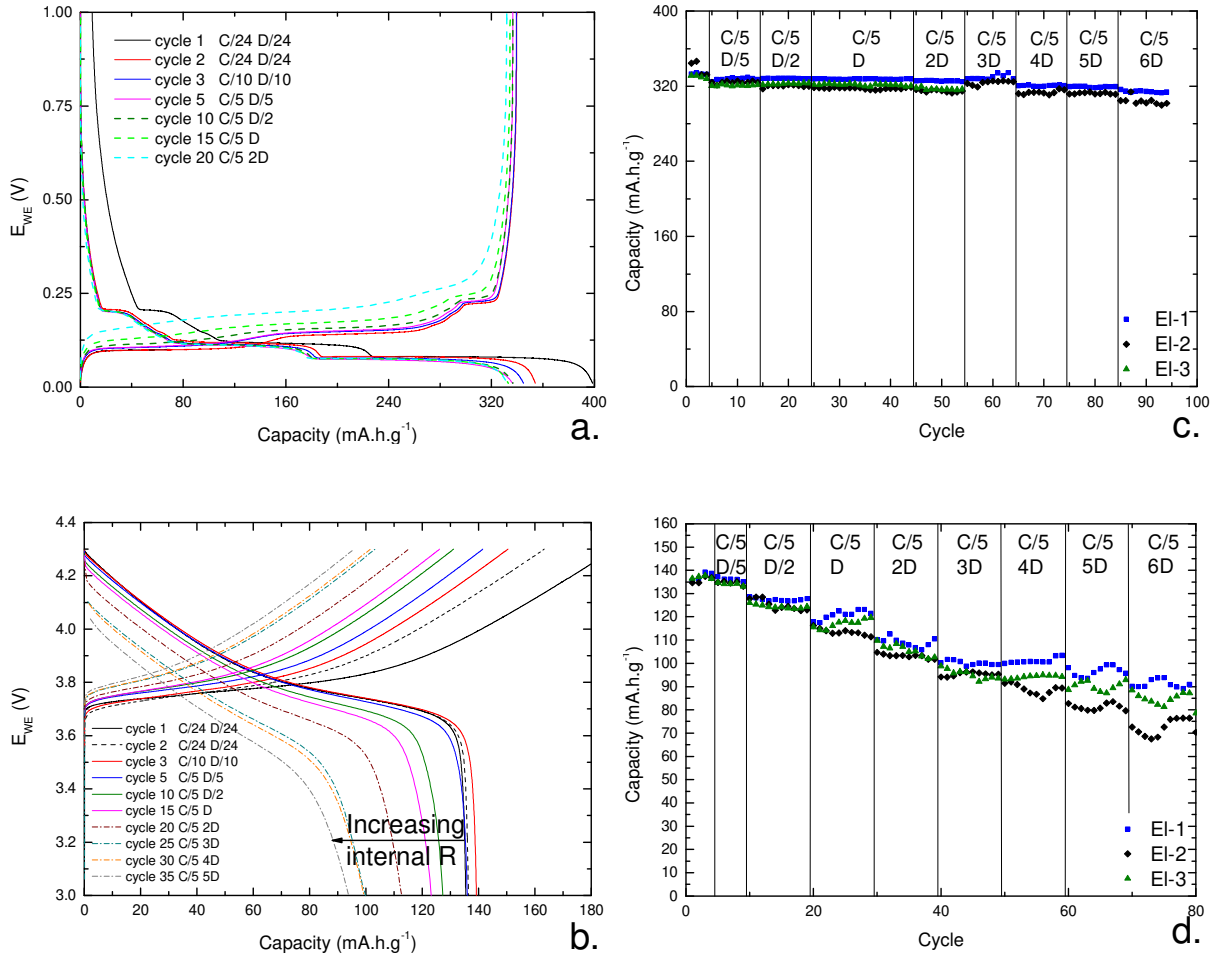

Figure 11. Charge/discharge profiles for (a) Gr/Li, and (b) NMC/Li half-cells containing El-1 as the electrolyte and capacity retention of the (c) Gr/Li, and (d) NMC/Li half-cells with the cycle number at different D-rates using El-1, El-2 and El-3 as electrolytes.

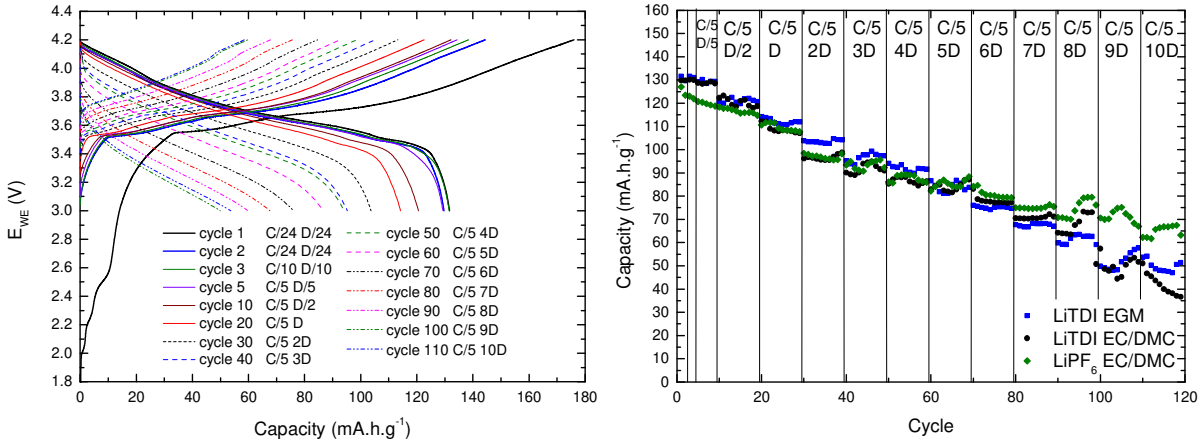

Figure 12. Charge/discharge curves of a NMC/Gr cell using El-1 as the electrolyte and NMC capacity retention in a NMC/Gr full-cell using the El-1, El-2 and El-3 electrolytes.

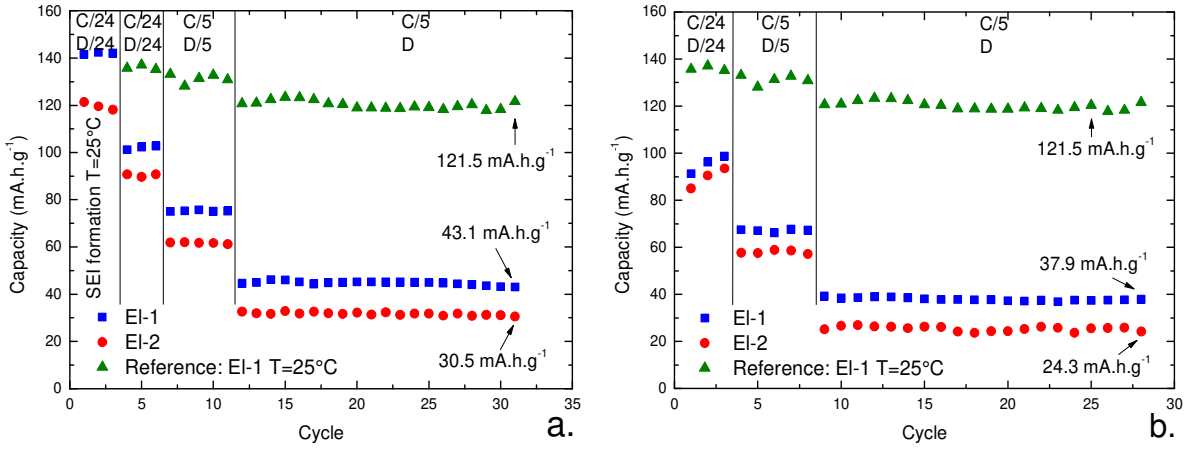

Figure 13. Discharge capacities at -20 °C of a NMC/Gr cell after SEI formation at (a) room temperature, and at (b) -20 °C. The electrolytes used are El-1 (blue squares) and El-2 (red discs). For comparison a NMC/Gr cell cycled at 25 °C using El-1 (green triangles) was added.

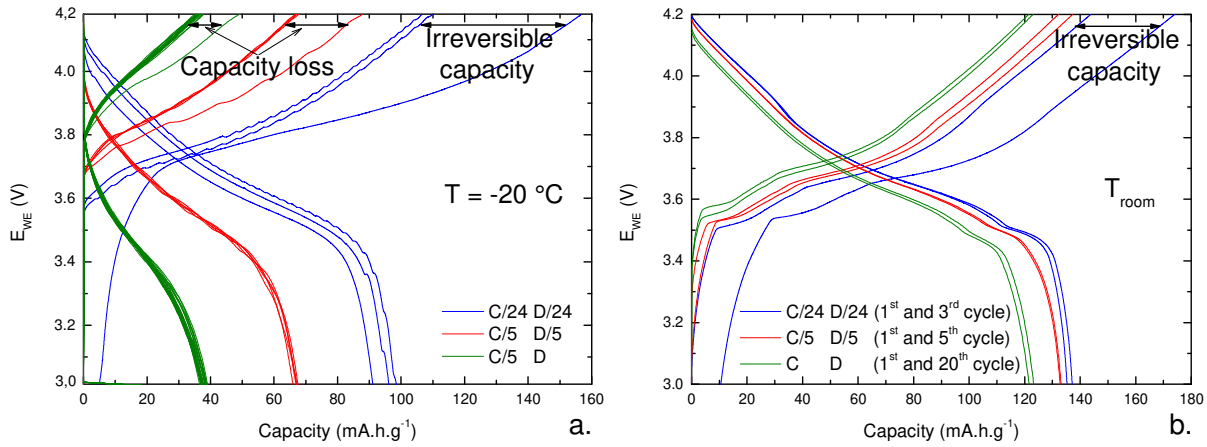

Figure 14. Charge/discharge plots obtained at (a) -20 °C, and at (b) room temperature (T_{room}). LiTDI-EGM+2%FEC was the electrolyte.

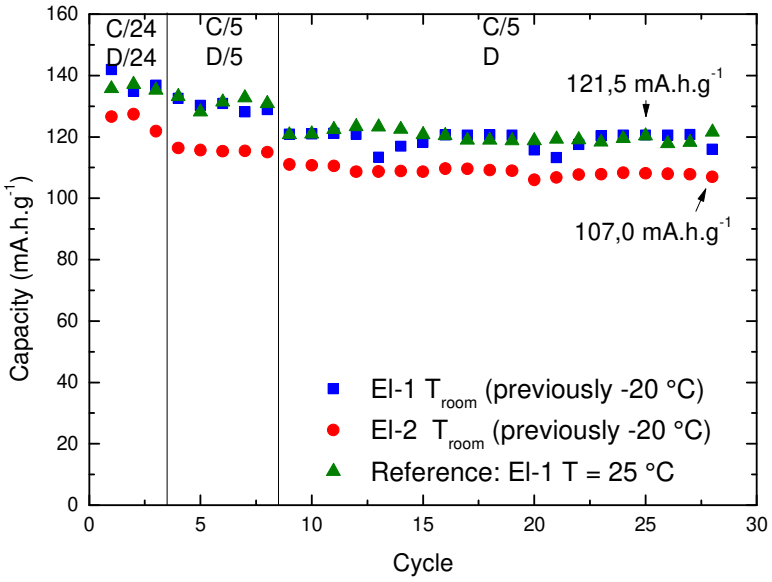

Figure 15. Room temperature discharge capacities of the NMC electrode previously cycled at -20 °C.

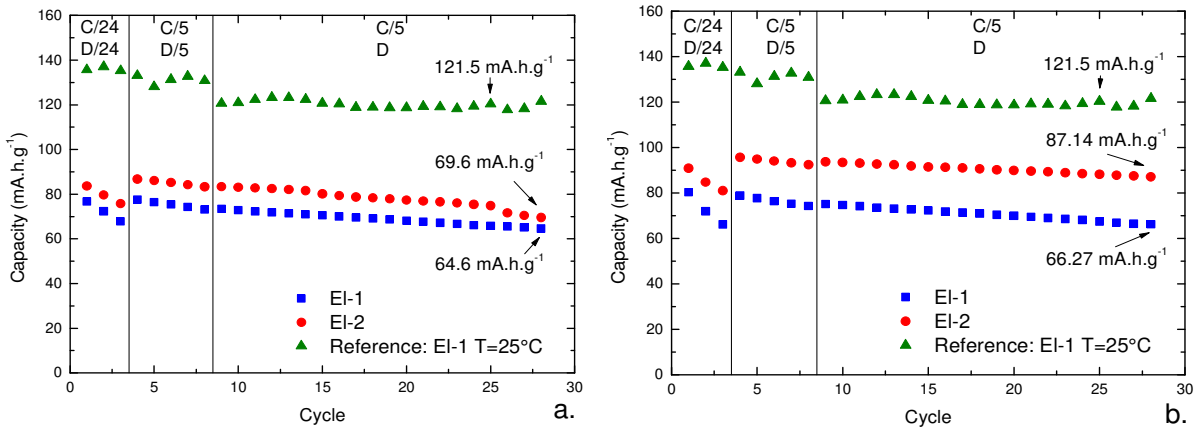

Figure 16. Discharge capacities of the NMC electrode at several charge/discharge rates obtained at 60 °C with (a) formation of the SEI at 60 °C, and (b) formation of the SEI at room temperature.

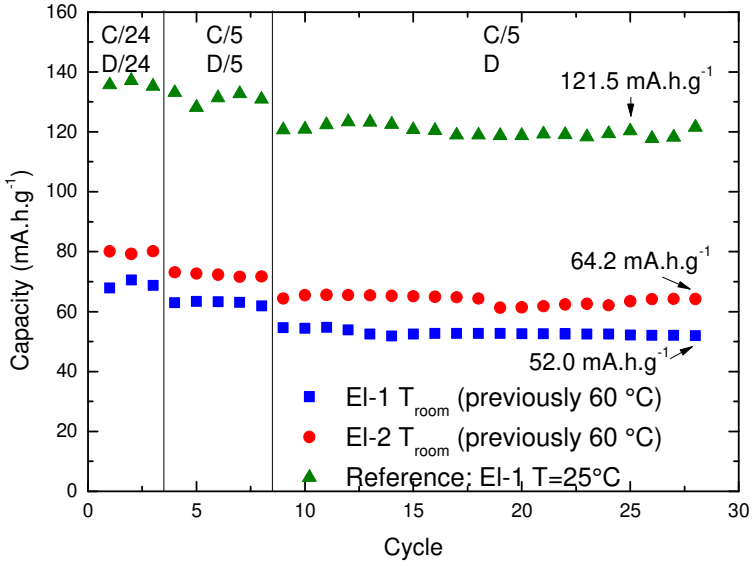

Figure 17. Room temperature discharge capacities of the NMC electrode previously cycled at 60 °C.

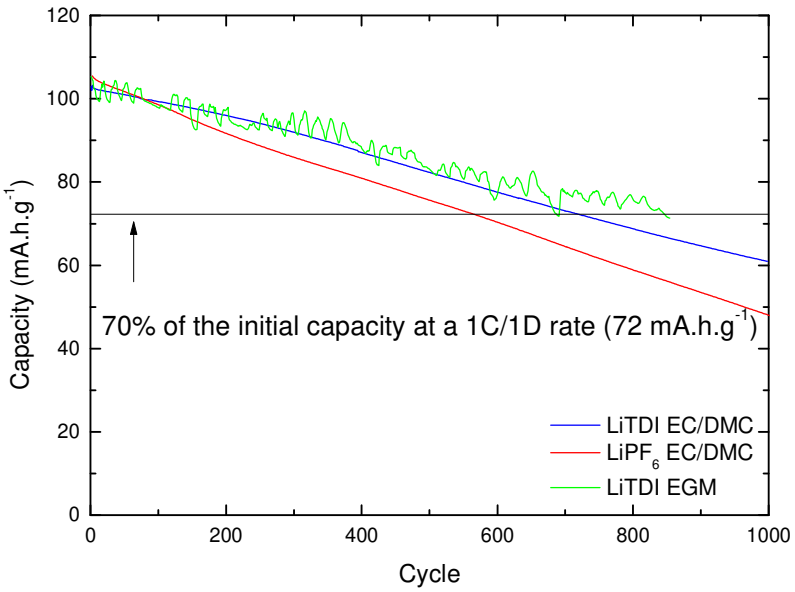

Figure 18. NMC/Gr cell durability test at a 1C charge/ 1D discharge rate obtained using the El-1, El-2 and El-3 electrolytes. Fluctuations observed in the case of El-1 are due to room temperature variations with time (one month).

Tables

Table 1. Melting temperature (T_m), boiling temperature (T_b), density at 25 °C (d_{25}), viscosity at 25 °C (η_{25}), dipolar moment (μ), relative permittivity (ε_r) and conductivity at 25 °C in the presence of LiTDI at 1 mol.L^{-1} (σ_{LiTDI}) of single solvents EC, GBL, MP [19] , DMC [21] and EGM and EC/DMC solvent mixtures.

	T_m (°C)	T_b (°C)	d_{25}	η_{25} (mPa.s)	μ (D)	ε_r	σ_{LiTDI} (mS.cm^{-1})
EC	36	248	1.32	solid	4.87	90	4.33
GBL	-44	204	1.12	1.7	4.12	39	7.66
MP	-88	80	0.91	0.5	1.8[20]	5.4	4.77
DMC	5	95	1.06	0.58	0.9	3.1	1.93
EC/GBL/MP	-48	130	1.16	1.08	/	58±5	8.32
EC/DMC	-23	130	1.20	1.10	/	43±5	6.11

Table 2. Irreversible capacities as a percentage of the initial charge capacity up to the 4th cycle for Gr/Li, NMC/Li half-cells and NMC/Gr full cells.

	Gr/Li			NMC/Li			NMC/Gr		
Cycle	2	3	4	2	3	4	2	3	4
El-1	8.90	1.92	0	13.16	4.48	2.40	13.78	5.02	2.94
El-2	9.06	0.22	0	13.29	4.93	2.35	13.36	6.21	2.87
El-3	7.85	1.46	1.21	19.32	3.30	2.12	22.12	6.11	0.91